atmosphere

Article

Morphology of Traveling Wave Disturbances Recorded in Eastern Siberia in 630 nm Atomic Oxygen Emission

Tatyana E. Syrenova *, Alexander B. Beletsky, Konstantin G. Ratovsky, Maxim V. Tolstikov and Roman V. Vasilyev

Institute of Solar-Terrestrial Physics SB RAS, 664033 Irkutsk, Russia; beletsky@iszf.irk.ru (A.B.B.); ratovsky@iszf.irk.ru (K.G.R.); maxim@iszf.irk.ru (M.V.T.); vasilyev@iszf.irk.ru (R.V.V.)
* Correspondence: angata@mail.iszf.irk.ru

Abstract: Our paper presents the results of investigating wave structures detected in 630 nm atomic oxygen emission intensity (airglow height is ~180–300 km). The study employs data from a wide-angle optical system installed at the Geophysical Observatory of the ISTP SB RAS (51°48′ N, 103°04′ E). It describes the algorithm to identify wave disturbances and determine their main parameters in the optical system images. The results obtained due to automatic processing of 2014–2021 data archives are presented. The most probable values of the wave disturbances propagation velocity are about 80 m/s. The horizontal wavelengths and periods are in the range of ~30–400 km and 60–120 min, respectively. The predominant direction of disturbances propagation is to the southwest. The received data of optical and radio observations are compared. We found both similarities and differences in the wavelike structures direction, which are to be investigated in the future.

Keywords: acoustic-gravity waves; all-sky camera; traveling ionospheric disturbances; atmospheric emission

check for updates

Citation: Syrenova, T.E.; Beletsky, A.B.; Ratovsky, K.G.; Tolstikov, M.V.; Vasilyev, R.V. Morphology of Traveling Wave Disturbances Recorded in Eastern Siberia in 630 nm Atomic Oxygen Emission. *Atmosphere* **2022**, *13*, 198. https://doi.org/10.3390/atmos13020198

Academic Editor: Guozhu Li

Received: 2 December 2021
Accepted: 25 January 2022
Published: 26 January 2022

1. Introduction

Wave disturbances in the Earth's atmosphere play a significant role, participating in dynamic processes. The first information about the relationship between periodic variations in the upper atmosphere emission parameters and atmospheric wave processes refer to the middle of the last century [1,2]. The authors of [3] were the first to detect wave structures caused by internal gravity waves (IGW) using all-sky cameras. More recent experimental and theoretical studies showed that, in reality, the main sources of periodic disturbances in the upper atmosphere are mainly acoustic-gravity waves (AGW) and IGWs. Sources of such disturbances might include meteorological processes, convection in the troposphere [4], geomagnetic activity [5], earthquakes [6], volcanoes, relief features, the passage of solar terminator [7], and the effects of anthropogenic activities, such as spacecraft launches, explosions, etc. These wave disturbances are energy carriers between different atmospheric layers and longitudinal–latitudinal regions. Therefore, it is important to study their basic parameters and behavior. One can use ground-based optical methods to observe wave structures of the upper atmosphere from airglow intensity variations. Additionally, radio methods using radars and ionosondes, e.g., [8–11] and GPS system [12–14] can be employed to observe these structures from traveling ionospheric disturbances (TID). Since the 1990s, all-sky cameras using high-sensitivity charge-coupled cooled devices have been widely used to observe disturbances in OI emission intensity (630.0 nm), e.g., [15,16]. Currently, observations with optical instruments cover almost all latitudes of both hemispheres, in such regions as Japan [17–20], China [21], Australia, Indonesia [22], India [23,24], Central and South America [25–27], Northern Europe [28], Canada [29], and North America [30].

Among many methods employed to detect wave disturbances and other inhomogeneities, wide-angle optical systems are more informative due to their wide viewing angle [17]. This field of view allows us to observe spatial scales of propagating disturbances and use a rather long series of observations. Such systems can be conveniently networked, e.g., [31,32], which makes it possible to observe large-scale concentric waves. In addition, spaced instruments using stereo vision allow obtaining the heights of events detected.

2. Materials and Methods

In this work, we used data from the KEO Sentinel wide-angle optical system, designed to record the spatial pattern of 630 nm emission intensity (airglow height is 180–300 km). The KEO Sentinel optical system is located in the ISTP SB RAS Geophysical Observatory near village Tory, Republic of Buryatia (52° N, 103° E, height 670 m). Full-width half-maximum of the interference filter is ~2 nm. The viewing direction is zenith, field of view is 145 degrees, exposure time is 30–60 s (http://atmos.iszf.irk.ru/ru/data/keo, (accessed on 1 December 2021).

For analysis, we selected data collected during clear-sky moonless nights from January 2014 to May 2021. Operator selected appropriate intervals by hand. The total number of nights selected for analysis is 112 (~770 h).

To obtain and assess the basic parameters of wave structures in KEO Sentinel images, we developed and tested an algorithm to automatically detect wave disturbances on images made with wide-angle cameras and obtain their characteristics. The algorithm includes several successive stages. In the first stage, we used a modified time differencing method (TD method) [33]. The idea of the processing algorithm is to plot the pattern of intensity differences between two consecutive frames. Figure 1 shows how the TD method is applied to consecutive images. First of all, we integrate the images received over a certain time interval. Next, pixel by pixel subtraction of two integrated frames is carried out. All stationary objects are eliminated, and the resulting frame presents the pattern of airglow spatial distribution. Then, two consecutive frames obtained as described above are again subtracted from each other for better contrast of the image irregularities. The spatial differencing enhances the contrast of both short-scale waves and larger scales.

Figure 2 shows the original contrast frame of the KEO Sentinel optical system (a) recorded on 05.01.2019 at 10.53.51 UT (18.53.51 LT) and the frame processed using the TD method (b). The frame projection onto the Earth's surface is made for the height of 630 nm airglow emission.

We use the algorithm for automatic alignment of the camera image pixels to geographic coordinates [34] to project the obtained images onto the Earth's surface (Figure 2b). It is necessary for correct assessment of spatial characteristics of the identified wave disturbances.

We determine longitudinal and transverse intensity profiles for each frame according to the coordinate grid in Figure 2b. Then, we calculate the functions of cross-correlation between each intensity profile and a set of reference signals. Reference signals represent two periods of harmonic oscillation of different spatial frequencies (0.002–0.1 km^{-1}). If the maximum of the cross-correlation function exceeds the 0.7 threshold, it is considered that a wave event with the frequency corresponding to that of the reference signal has been identified. Cross-correlational functions with maximum values under 0.7 further lead to unstable performance of the algorithm for automatic estimation of wave disturbance parameters.

For each wave event found, we determine the wavefront and its propagation azimuth (Figure 3). Then, we identify the image area where the disturbance is detected and calculate its true frequency. When calculating the frequency values, the algorithm takes into account the wavelength distortion introduced by the TD method. When the same frequency of disturbances is revealed in the same image area, these disturbances in two adjacent frames are combined into one event.

The cross-correlation function of temporal dynamics of the revealed wave disturbance for the frames obtained at different times is used to estimate the disturbance velocity and propagation direction.

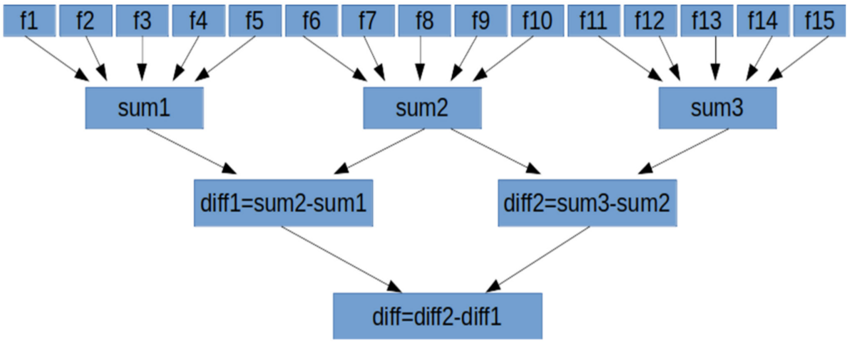

Figure 1. Example of TD method application.

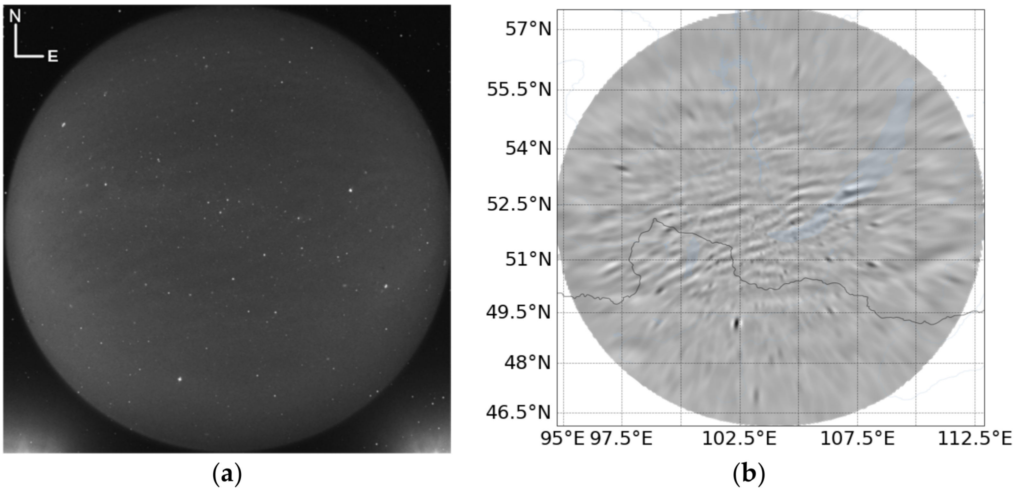

Figure 2. Example KEO Sentinel frame on 05.01.2019, 10:53 UT (18.53 LT): (**a**) original frame; and (**b**) after applying the TD method. The image projection is made for the height of 250 km.

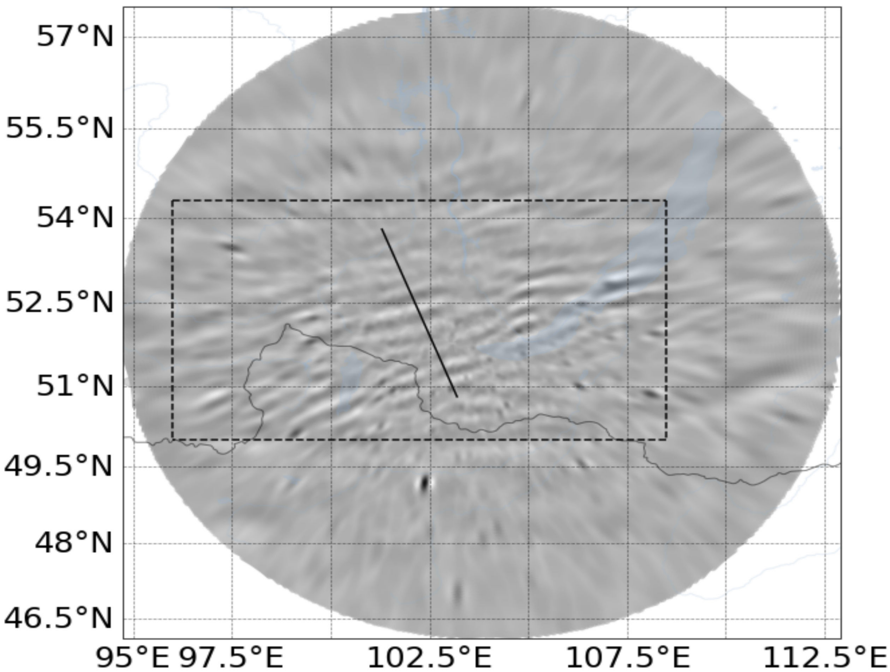

Figure 3. Example areas indicated by rectangles with detected disturbances and determined front inclinations.

3. Results

To compare the results of processing the observed periodic structures with data on wave disturbances obtained using the means of radio research [35], we should move to time characteristics. Knowing the spatial frequency of the wave disturbance and its propagation velocity, one can determine its time periodicity in a trivial way. We divided the received wave disturbances into three groups defined as follows: short-period—up to 20 min, medium-period—from 20 to 60 min, and long-period—from 60 min. Figures 4–6 show the resultant statistical distributions of parameters of different periodic disturbances for all seasons in 2014–2021. Summer months are not included, as there is little data in summer due to short and mostly light nights. Therefore, we mainly took the data for late autumn, winter and spring. According to this data, the seasonal dependence, which must be present, has not yet been possible to track.

According to the processing results, the prevailing direction of propagation of short-period disturbances is southwest and, to a lesser extent, east (Figure 4b). The horizontal wavelength of these disturbances is 35–50 km, and their horizontal velocity averages 70–80 m/s.

For medium-period disturbances, two basic directions are revealed: south and south-west (Figure 5b). At the same time, their velocities are mainly 80 m/s, periods are ~25–30 min, and horizontal wavelength is ~140–160 km. The azimuths of long-period disturbances have three main directions—south, southwest and southeast, propagation velocities are slightly lower—40 m/s, periods are mainly ~100 min, horizontal wavelength ranges from 200 to 300 km.

For all seasons, the disturbances are mainly of southwest direction.

We compared the obtained optical data with the characteristics of night traveling ionospheric disturbances (TID) according to data from the ISTP SB RAS Radio Physical Complex (Figure 6). To compare optical data, we chose long-period disturbances since they are closest to the periods observed using radio methods. The average velocities of disturbance propagation are similar comprising ~80 m/s. Typical velocities of night mid-latitude TIDs obtained in different studies are also within 50–100 m/s, and their periods are 0.5–1.5 h on average, horizontal wavelengths are 100–400 km [17,27,36–39].

According to radio data, there are two most probable TID azimuths—about 240 degrees (southwest direction) and about 0/360 degrees (north). According to optical data with close periods, directions for wave disturbances are about 250 degrees, northern directions are not observed.

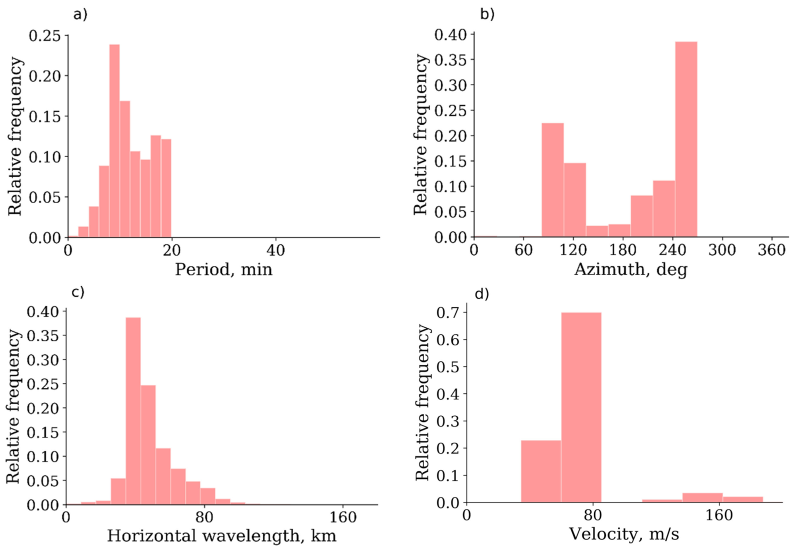

Figure 4. Distributions of parameters of short-period traveling wave disturbances from KEO Sentinel data: periods (**a**), azimuth (**b**), horizontal wavelength (**c**) and horizontal velocity (**d**).

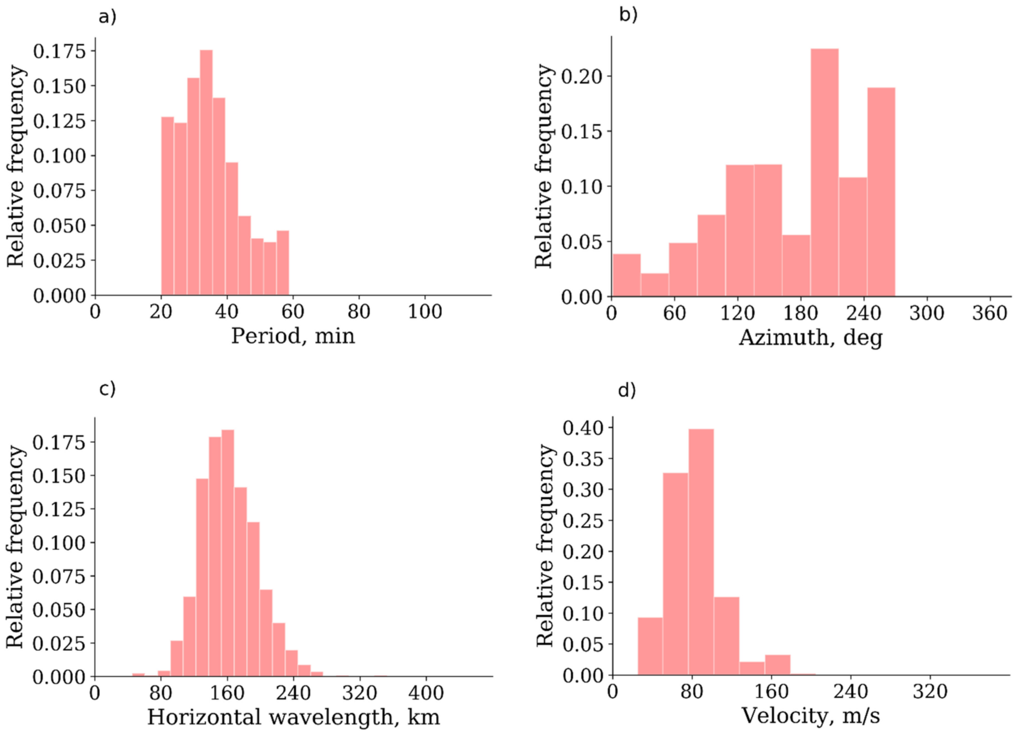

Figure 5. Distributions of parameters of medium-period traveling wave disturbances from KEO Sentinel data: periods (**a**), azimuth (**b**), horizontal wavelength (**c**) and horizontal velocity (**d**).

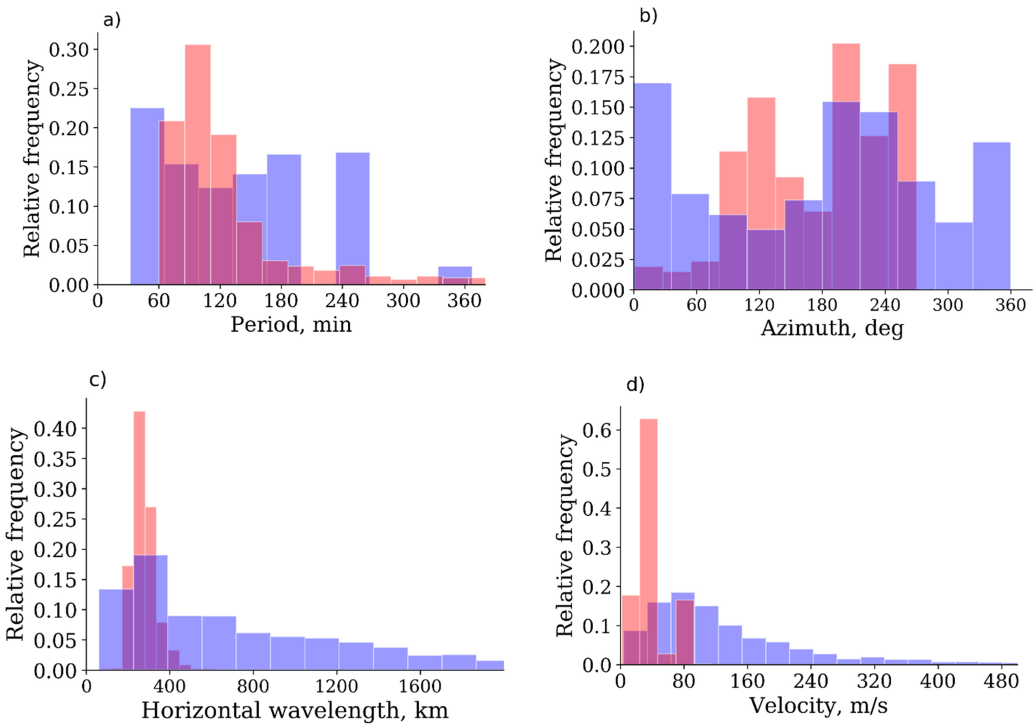

Figure 6. Distributions of TID parameters from the Radio Physical Complex data (blue bars) and disturbances from optical data (red bars): periods (**a**), azimuth (**b**), horizontal wavelength (**c**) and horizontal velocity (**d**).

4. Discussion

At present, there is a fairly large volume of wave disturbance studies carried out with using various methods in different latitudinal-longitudinal regions of the Earth. There are nighttime mid-latitude MS TIDs, their parameters do not fit into the classical theory of IGW propagation [40]. To explain such MS TIDs, electrodynamic processes are involved, in particular, the Perkins instability [17,37,38]. It is known that there is a latitudinal dependence of the disturbance parameters. For example, Fedorenko et al. [41] showed such a dependence for the F-layer heights. Nevertheless, at the latitudes of our observation point (52 N) detailed studies of nighttime MS TIDs using optical methods were carried out only in Japan. Other statistically significant observations were carried out at lower latitudes, which may affect the nighttime MS TIDs behavior [40]. Therefore, it is important to obtain the traveling wave disturbances morphology in the upper atmosphere for different longitudinal sectors.

According to the Radio Physical Complex data, the prevailing directions of wave disturbances propagation are to the southwest and north, while the optical data mainly show the southwest and southeast directions. Disturbances directed to the equator in both hemispheres were obtained in many researches carried out by studying the variations of different parameters [15,17,21,26,28,39,42–52]. The direction of wave disturbances motion to the north was obtained from the radio physical data, which is not observed in the optical data and in the data of studies carried out in other longitudinal sectors.

The radio technique used by us allows obtaining characteristics of mainly large-scale TIDs with periods larger than ~45 min and horizontal wave lengths larger than ~100 km without limitation for long wavelengths. The optical equipment and method we use allows obtaining characteristics of disturbances with shorter periods and wavelengths compared to the radio technique, but at present the optical technique is limited by the maximal horizontal wave length of ~500 km. In addition to the limitations of the methods described, there may be physical reasons for the differences between the results of radio and optical methods. Physical reasons can be associated with different manifestations of wave disturbances in airglow and electron density. For example, the optical data give the preferable south-west direction for propagation of nighttime TIDs while the radio data show the presence of northward nighttime TIDs (e.g., see the Hocke and Schlegel review [53] and references therein, or the studies of Medvedev et al. [10,35,54]. The explanation for this difference is an open question and requires further research.

Medvedev et al. [54] checked the dispersion relation for IGWs and it was shown that ~50% of winter nighttime TIDs are IGW manifestations. The rest of the nighttime TIDs (~50%) can be related to plasma instabilities, such as the Perkins instability [51]. In this paper, we do not measure the total TID velocity vector and, therefore, cannot directly check the dispersion relation. However, we can test the IGW wind filtration hypothesis with using representative statistics. When the IGWs propagate downwind, the IGW amplitude decreases significantly due to dissipation, while the IGWs propagate upwind, the IGW amplitude increases [55–57]. In the study of Pogoreltsev and Pertsev [55], an increase or decrease in the IGW amplitude due to wind influence is the result of the numerical simulation without explaining the mechanism. In the studies of Waldock and Jones [56,57], a decrease in the IGW amplitude due to wind influence is a hypothesis that explains the suppression of waves travelling with a component in the wind direction. An alternative explanation of the wind filtration hypothesis was given by Shiokawa et al. [58] when gravity waves propagate downwind, its vertical wavelength becomes small so that the airglow perturbations caused by the gravity waves could be smeared out. Thus, the observation probability increases for IGW propagating in the direction opposite to the neutral wind acting at the observation altitude. On the contrary, in the direction coinciding with a strong neutral wind (more than 50 m/s) at any of the heights through which the IGW passed before reaching the observation altitude, the propagation of the IGW is blocked. Therefore, for most IGWs, the projection of the neutral wind on the direction of propagation should be negative. Waldock and Jones [56,57], Kalikhman [59], and Crowley et al. [60] revealed that most TIDs are observed in the cases when the TID propagation direction is near antiparallel to the background neutral wind velocity. The explanation of this effect (so-called wind-filtering hypothesis) lies in that the downwind propagation strongly reduces the IGW amplitude due to dissipation, while the upwind propagation slightly enhances the amplitude [55–57]. Therefore, if TIDs are IGWs manifestation, then the TIDs azimuths distribution is determined by the seasonal and diurnal neutral wind distribution. Studies [11,54,61] concluded that the azimuth preferences may be caused by wind filtering. For the Irkutsk night, according to HWM2007, most IGW azimuths should lie in the ranges of ~0–30° and ~210–360° [54]. This range of azimuths contains ~40% of the disturbances. Thus, according to indirect data, it can be argued that ~40% of winter nocturnal TIDs are manifestations of IGW, which is comparable to the estimation of ~50% made by Medvedev et al. [54].

5. Conclusions

For the first time, for the Asian part of Eurasia, the statistical parameters of nighttime wave disturbances recorded in the 630 nm emission intensity (altitude about 250 km) were obtained using a wide-angle camera.

The automatic algorithm applied makes it possible to successfully distinguish periodic structures in the images of a wide-angle system and obtain their main characteristics. In addition, the automated procedure significantly reduces the time of processing archive and current data. The main parameters of large-scale wave disturbances from optical data that were obtained after processing using the algorithm are in good agreement with data from the Radio Physical Complex. The most probable velocities of propagation of all-scale wave disturbances, resulting from automatic processing, are about 80 m/s. Horizontal wavelengths of short-period disturbances are 30–40 km, those of medium- and long-period disturbances are 150–160 and 20–300 km, respectively. Periods of disturbances average 60–120 min. The observed disturbances propagate mostly southwest. Yet, the optical data report on additional directions—southeast and south, but no north direction, which is detected in radio data.

The received directions of the southwest of the wave disturbances confirm the global feature in observations for the Northern Hemisphere mid-latitudes seen by many researchers who also used data of 630 nm emission optical observations and radio methods. Further extended work is needed on the processing of archive and current optical data and their comparison with radio data. This will make it possible to identify the most probable mechanism for the generation of wave disturbances and their relation to night MS TIDs in the mesosphere and lower thermosphere at mid-latitudes, to try to explain the similarities and differences found in the directions of disturbances propagation

Author Contributions: Software, data analysis and visualization, A.B.B., T.E.S., K.G.R., M.V.T., writing review and editing, T.E.S., K.G.R., A.B.B., conceptualization, methodoloy and project administration, A.B.B., R.V.V. All authors provided critical feedback and helped shape the research, analysis and manuscript. All authors have read and agreed to the published version of the manuscript.

Funding: The work was financially supported by the Ministry of Science and Higher Education of the Russian Federation (Subsidy №075-GZ/C3569/278) and by RFBR (grant №20-05-00580).

Institutional Review Board Statement: Not applicable.

Informed Consent Statement: Not applicable.

Data Availability Statement: KEO Sentinel data from http://atmos.iszf.irk.ru/ru/data/keo (accessed on 1 December 2021) and Unique Research Facility "Irkutsk Incoherent Scatter Radar" (http://ckp-rf.ru/usu/77733/, accessed on 1 December 2021).

Acknowledgments: The results were obtained using the equipment of Shared Equipment Center "Angara" (http://ckp-rf.ru/ckp/3056/, accessed on 1 December 2021) and the Unique Research Facility "Irkutsk Incoherent Scatter Radar" (http://ckp-rf.ru/usu/77733/, accessed on 1 December 2021).

Conflicts of Interest: The authors declare no conflict of interest.

References

1. Krassovsky, V.I. Nature of intensity variations of the terrestrial atmosphere emission. *Liege Int. Astrophys. Colloq.* **1957**, *18*, 58–67.
2. Krassovsky, V.I. Priroda izmenenii intensivnosti emissii zemnoy atmosfery. *Izv. AN SSSR. Ser.geofiz.* **1957**, *5*, 664–669. (In Russian)
3. Taylor, M.J.; Hapgood, M.A. On the origin of ripple-type wave structure in the nightglow emission. *Planet. Space Sci.* **1990**, *38*, 1421–1430. [CrossRef]
4. Borchevkina, O.P.; Korenkova, N.A.; Karpov, I.V.; Vlasov, V.I.; Karpov, M.I.; Leshchenko, V.S. Impact of meteorological storms on the E-region of the ionosphere in 2017–2018. *Sol.-Terr. Phys.* **2021**, *6*, 74–79.
5. Medvedev, A.V.; Ratovsky, R.V.; Tolstikov, M.V.; Scherbakov, A.A.; Alsatkin, S.S. Statisticheskoe issledovanie charakteristik rasprostraneniya peremeschayuschihsya ionosfernyh vozmuscheniy po dannym radiofizicheskogo kompleksa ISZf SO RAN. *Solnechno-Zemn. Fiz.* **2012**, *20*, 85–91. (In Russian)
6. Piersanti, M.; Materassi, M.; Battiston, R.; Carbone, V.; Cicone, A.; D'Angelo, G.; Diego, P.; Ubertini, P. Magnetospheric–Ionospheric–Lithospheric Coupling Model. 1: Observations during the 5 August 2018 Bayan Earthquake. *Remote Sens.* **2020**, *12*, 3299. [CrossRef]
7. Somsikov, V.M. Volny v atmosfere, obuslovlennye solnechnym terminatorom. *Geomagn. I Aeron.* **1991**, *31*, 1–12. (In Russian)
8. Nicolls, M.J.; Heinselman, C.J. Three-dimensional measurements of traveling ionospheric disturbances with the Poker Flat Incoherent Scatter Radar. *Geophys. Res. Lett.* **2007**, *34*, L21104. [CrossRef]
9. Ratovsky, K.G.; Medvedev, A.V.; Tolstikov, M.V.; Kushnarev, D.S. Case studies of height structure of TID propagation characteristics using cross-correlation analysis of incoherent scatter radar and DPS-4 ionosonde data. *Adv. Space Res.* **2008**, *41*, 1453–1457. [CrossRef]
10. Medvedev, A.V.; Ratovsky, K.G.; Tolstikov, M.V.; Alsatkin, S.S.; Scherbakov, A.A. Studying of the spatial-temporal structure of wavelike ionospheric disturbances on the base of Irkutsk Incoherent Scatter Radar and Digisonde data. *J. Atmos. Sol.-Terr. Phys.* **2013**, *105–106*, 350–357. [CrossRef]
11. Oinats, A.V.; Kurkin, V.I.; Nishitani, N. Statistical study of medium-scale traveling ionospheric disturbances using SuperDARN Hokkaido ground backscatter data for 2011. *Earth Planets Space* **2015**, *67*, 22.
12. Afraimovich, E.L.; Kosogorov, E.A.; Lesyuta, O.S.; Ushakov, I.I.; Yakovets, A.F. Geomagnetic control of the spectrum of traveling ionospheric disturbances based on data from a global GPS network. *Ann. Geophys.* **2001**, *19*, 723–731. [CrossRef]
13. Afraimovich, E.L.; Voeykov, S.V.; Perevalova, N.P.; Ratovsky, K.G. Large-scale traveling ionospheric disturbances of auroral origin according to the data of the GPS network and ionosondes. *Adv. Space Res.* **2008**, *42*, 1213–1217. [CrossRef]
14. Otsuka, Y.; Kotake, N.; Shiokawa, K.; Ogawa, T.; Tsugawa, T.; Saito, A. Statistical study of medium-scale traveling ionospheric disturbances observed with a GPS receiver network in Japan. In *Aeronomy of the Earth's Atmosphere and Ionosphere*; Abdu, M., Pancheva, D., Bhattacharyya, A., Eds.; IAGA Special Sopron Book Series; Springer: Dordrecht, The Netherlands, 2011; Volume 2, pp. 291–299.
15. Mendillo, M.; Baumgardner, J.; Nottingham, D.; Aarons, J.; Reinisch, B.; Scali, J.; Kelley, M. Investigations of thermospheric-ionospheric dynamics with 6300 A images from the Arecibo Observatory. *J. Geophys. Res.* **1997**, *102*, 7331–7343. [CrossRef]
16. Taylor, M.J.; Jahn, J.-M.; Fukao, S.; Saito, A. Possible evidence of gravity wave coupling into the mid-latitude F region ionosphere during the SEEK campaign. *Geophys. Res. Lett.* **1998**, *25*, 1081–1084. [CrossRef]
17. Shiokawa, K.; Ihara, C.; Otsuka, Y.; Ogawa, T. Statistical study of nighttime medium-scale traveling ionospheric disturbances using midlatitude airglow images. *J. Geophys. Res.* **2003**, *108*, 1052. [CrossRef]
18. Shiokawa, K.; Otsuka, Y.; Ogawa, T. Propagation characteristics of nighttime mesospheric and thermospheric waves observed by optical mesosphere thermosphere imagers at middle and low latitudes. *Earth Planets Space* **2009**, *61*, 479–491. [CrossRef]
19. Otsuka, Y.; Shiokawa, K.; Ogawa, T.; Wilkinson, P. Geomagnetic conjugate observations of medium-scale traveling ionospheric disturbances at midlatitude using all-sky airglow imagers. *Geophys. Res. Lett.* **2004**, *31*, L15803. [CrossRef]
20. Tsuchiya, S.; Shiokawa, K.; Fujinami, H.; Otsuka, Y.; Nakamura, T.; Yamamoto, M. Statistical analysis of the phase velocity distribution of mesospheric and ionospheric waves observed in airglow images over a 16-year period: Comparison between Rikubetsu and Shigaraki, Japan. *J. Geophys. Res. Space Phys.* **2018**, *123*, 6930–6947. [CrossRef]
21. Li, Q.; Xu, J.; Yue, J.; Yuan, W.; Liu, X. Statistical characteristics of gravity wave activities observed by an OH airglow imager at Xinglong, in northern China. *Ann. Geophys.* **2011**, *29*, 1401–1410. [CrossRef]
22. Fukushima, D.; Shiokawa, K.; Otsuka, Y.; Ogawa, T. Observation of equatorial nighttime medium-scale traveling ionospheric disturbances in 630-nm airglow images over 7 years. *J. Geophys. Res.* **2012**, *117*, a10324. [CrossRef]
23. Parihar, N.; Taori, A. An investigation of long-distance propagation of gravity waves under CAWSES India Phase II Programme. *Ann. Geophys.* **2015**, *33*, 547–560. [CrossRef]
24. Ramkumar, T.K.; Malik, M.A.; Ganaie, B.A.; Bhat, A.H. Airglow-imager based observation of possible influences of subtropical mesospheric gravity waves on F-region ionosphere over Jammu & Kashmir, India. *Sci Rep.* **2021**, *11*, 10168.
25. Vadas, S.L.; Liu, H. Generation of large-scale gravity waves and neutral winds in the thermosphere from the dissipation of convectively generated gravity waves. *J. Geophys. Res.* **2009**, *114*, A10310. [CrossRef]
26. Essien, P.; Paulino, I.; Wrasse, C.M.; Campos, J.A.V.; Paulino, A.R.; Medeiros, A.F.; Buriti, R.A.; Takahashi, H.; Agyei-Yeboah, E.; Lins, A.N. Seasonal characteristics of small- and medium-scale gravity waves in the mesosphere and lower thermosphere over the Brazilian equatorial region. *Ann. Geophys.* **2018**, *36*, 899–914. [CrossRef]

27. Paulino, I.; Medeiros, A.F.; Vadas, S.L.; Wrasse, C.M.; Takahashi, H.; Buriti, R.A.; Leite, D.; Filgueira, S.; Bageston, J.V.; Sobral, J.H.A.; et al. Periodic waves in the lower thermosphere observed by OI630 nm airglow images. *Ann. Geophys.* **2016**, *34*, 293–301. [CrossRef]
28. Otsuka, Y.; Suzuki, K.; Nakagawa, S.; Nishioka, M.; Shiokawa, K.; Tsugawa, T. GPS observations of medium-scale traveling ionospheric disturbances over Europe. *Ann. Geophys.* **2013**, *31*, 163–172. [CrossRef]
29. Suzuki, S.; Shiokawa, K.; Hosokawa, K.; Nakamura, K.; Hocking, W.K. Statistical characteristics of polar cap mesospheric gravity waves observed by an all-sky airglow imager at Resolute Bay, Canada. *J. Geophys. Res.* **2009**, *114*, A01311. [CrossRef]
30. Tsugawa, T.; Otsuka, Y.; Coster, A.J.; Saito, A. Medium-scale traveling ionospheric disturbances detected with dense and wide TEC maps over North America. *Geophys. Res. Lett.* **2007**, *34*, L22101. [CrossRef]
31. Xu, J.; Li, Q.; Yue, J.; Hoffmann, L.; Straka, W.C.; Wang, C.; Liu, M.; Yuan, W.; Han, S.; Miller, S.D.; et al. Concentric gravity waves over northern China observed by an airglow imager network and satellites. *J. Geophys. Res. Atmos.* **2015**, *120*, 11058–11078. [CrossRef]
32. Nishioka, M.; Tsugawa, T.; Kubota, M.; Ishii, M. Concentric waves and short-period oscillations observed in the ionosphere after the 2013 Moore EF5 tornado. *Geophys. Res. Lett.* **2013**, *40*, 5581–5586. [CrossRef]
33. Swenson, G.R.; Mende, S.B. OH emission and gravity waves (including a breaking wave) in all-sky imagery from Bear Lake, UT. *Geophys. Res. Lett.* **1994**, *21*, 2239–2242. [CrossRef]
34. Syrenova, T.E.; Beletsky, A.B.; Vasilyev, R.V. Geograficheskaya privyazka kadrov shirokougolnyh system. *J. Teh. Fiz.* **2021**, *91*, 1990–1996. (In Russian)
35. Medvedev, A.V.; Ratovsky, K.G.; Tolstikov, M.V.; Alsatkin, S.S.; Shcherbakov, A.A. A statistical study of internal gravity waves characteristics using the combined Irkutsk Incoherent Scatter Radar and Digisonde data. *J. Atmos. Sol.-Terr. Phys.* **2015**, *132*, 13–21. [CrossRef]
36. Garcia, F.J.; Kelley, M.C.; Makela, J.J.; Huang, C.-S. Airglow observations of mesoscale low-velocity traveling ionospheric disturbances at midlatitudes. *J. Geophys. Res.* **2000**, *105*, 18407–18415. [CrossRef]
37. Kubota, M.; Shiokawa, K.; Ejiri, M.K.; Otsuka, Y.; Ogawa, T.; Sakanoi, T.; Fukunishi, H.; Yamamoto, M.; Fukao, S.; Saito, A. Traveling ionospheric disturbances observed in the OI 630-nm nightglow images over Japan by using a multi-point imager network during the FRONT campaign. *Geophys. Res. Lett.* **2000**, *24*, 4037–4040. [CrossRef]
38. Kubota, M.; Fukunishi, H.; Okano, S. Characteristics of medium- and large-scale TIDs over Japan derived from OI 630-nm nightglow observation. *Earth Planets Space* **2001**, *53*, 741–751. [CrossRef]
39. Huang, F.; Dou, X.; Lei, J.; Lin, J.; Ding, F.; Zhong, J. Statistical analysis of nighttime medium-scale traveling ionospheric disturbances using airglow images and GPS observations over central China. *J. Geophys. Res.* **2016**, *121*, 8887–8899. [CrossRef]
40. Perevalova, N.P.; Oinats, A.V. *Morfologiya Nochnyh Peremeshchayushchihsya Ionosfernyh Vozmushcheniy v Sredneshirotnoy Oblasti F (Obzor Sovremennyh Predstavleniy)*; IGU: Irkutsk, Russia, 2020; p. 83. (In Russian)
41. Fedorenko, A.K.; Bespalova, A.V.; Zhuk, I.T.; Kryuchkov, E.I. Latitude variability of acoustic-gravity waves in the upper atmosphere based on satellite data. *Geomagn. Aeron.* **2017**, *57*, 471–481. [CrossRef]
42. Ejiri, M.K.; Shiokawa, K.; Ogawa, T.; Igarashi, K.; Nakamura, T.; Tsuda, T. Statistical study of short-period gravity waves in OH and OI nightglow images at two separated sites. *J. Geophys. Res.* **2003**, *108*, 4679. [CrossRef]
43. Kotake, N.; Otsuka, Y.; Tsugawa, T.; Ogawa, T.; Saito, A. Statistical study of medium-scale traveling ionospheric disturbances observed with the GPS networks in Southern California. *Earth Planets Space* **2007**, *59*, 95–102. [CrossRef]
44. Ding, F.; Wan, W.; Liu, L.; Afraimovich, E.L.; Voeykov, S.V.; Perevalova, N.P. A statistical study of large-scale traveling ionospheric disturbances observed by GPS TEC during major magnetic storms over the years 2003–2005. *J. Geophys. Res. Space Phys.* **2008**, *113*, A3. [CrossRef]
45. Chen, G.; Zhou, C.; Liu, Y.; Zhao, J.; Tang, Q.; Wang, X.; Zhao, Z. A statistical analysis of medium-scale traveling ionospheric disturbances during 2014–2017 using the Hong Kong CORS network. *Earth Planets Space* **2019**, *71*, 52.
46. Saito, A.; Fukao, S.; Miyazaki, S. High resolution mapping of TEC perturbations with the GSI GPS network over Japan. *Geophys. Res. Lett.* **1998**, *25*, 3079–3082. [CrossRef]
47. Saito, A.; Nishimura, M.; Yamamoto, M.; Fukao, S.; Kubota, M.; Shiokawa, K.; Otsuka, Y.; Tsugawa, T.; Ogawa, T.; Ishii, M.; et al. Traveling ionospheric disturbances detected in the FRONT campaign. *Geophys. Res. Lett.* **2001**, *28*, 689–692. [CrossRef]
48. Ogawa, T.; Igarashi, K.; Aikyo, K.; Maeno, H. NNSS satellite observations of medium-scale traveling ionospheric disturbances at southern high-latitudes. *J. Geomagn. Geoelectr.* **1987**, *39*, 709–721. [CrossRef]
49. Kelley, M.C.; Makela, J.J. Resolution of the discrepancy between experiment and theory of midlatitude F-region structures. *Geophys. Res. Lett.* **2001**, *28*, 2589–2592.
50. Behnke, R. F layer height bands in the nocturnal ionosphere over Arecibo. *J. Geophys. Res.* **1979**, *84*, 974–978. [CrossRef]
51. Perkins, F.W. Spread F and ionospheric currents. *J. Geophys. Res.* **1973**, *78*, 218–226. [CrossRef]
52. Makela, J.J.; Miller, E. S, Talaat, E.R. Nighttime medium-scale traveling ionospheric disturbances at low geomagnetic latitudes. *Geophys. Res. Lett.* **2010**, *37*, L24104. [CrossRef]
53. Hocke, K.; Schlegel, K. A review of atmospheric gravity waves and travelling ionospheric disturbances: 1982–1995. *Ann. Geophys.* **1996**, *14*, 917–940.
54. Medvedev, A.V.; Ratovsky, K.G.; Tolstikov, M.V.; Oinats, A.V.; Alsatkin, S.S.; Zherebtsov, G.A. Relation of internal gravity wave anisotropy with neutral wind characteristics in the upper atmosphere. *J. Geophys. Res. Space Phys.* **2017**, *122*, 7567–7580. [CrossRef]

55. Pogoreltsev, A.I.; Pertsev, N.N. The influence of background wind on the formation of the acoustic-gravity wave structure in the thermosphere. *Izv. Atmos. Ocean. Phys.* **1996**, *132*, 723–728.
56. Waldock, J.A.; Jones, T.B. The effects of neutral winds on the propagation of medium-scale atmospheric gravity wave at midlatitudes. *J. Atmos. Terr. Phys.* **1984**, *46*, 217–231. [CrossRef]
57. Waldock, J.A.; Jones, T.B. HF Doppler observations of medium-scale traveling ionospheric disturbances at mid-latitudes. *J. Atmos. Terr. Phys.* **1986**, *48*, 245–260. [CrossRef]
58. Shiokawa, K.; Otsuka, Y.; Ihara, C.; Ogawa, T.; Rich, F.J. Ground and satellite observations of nighttime medium-scale traveling ionospheric disturbance at midlatitude. *J. Geophys. Res.* **2003**, *108*, 1145. [CrossRef]
59. Kalikhman, A.D. Medium-scale traveling ionospheric disturbances and thermospheric winds in the F-region. *J. Atmos. Sol. Terr. Phys.* **1980**, *42*, 697–703. [CrossRef]
60. Crowley, G.; Jones, T.B.; Dudeney, J.R. Comparison of short period TID morphologies in Antarctica during geomagnetically quiet and active intervals. *J. Atmos. Terr. Phys.* **1987**, *49*, 1155–1162. [CrossRef]
61. Tolstikov, M.V.; Oinats, A.V.; Medvedeva, I.V.; Medvedev, A.V.; Ratovsky, K.G.; Nishitani, N. Relation of traveling ionospheric disturbances characteristics with planetary waves in the middle atmosphere. In Proceedings of the 2019 PhotonIcs & Electromagnetics Research Symposium-Spring (PIERS-Spring), Rome, Italy, 17–20 June 2019; pp. 2176–2182.